High Electrical Conductivity in Ni_3(2,3,6,7,10,11-hexaiminotriphenylene)$_2$, a Semiconducting Metal-Organic Graphene Analogue

Supporting Information

Dennis Sheberla,[†] Lei Sun,[†] Martin A. Blood-Forsythe,[‡] Süleyman Er, [‡] Casey R. Wade,[†] Carl K. Brozek,[†] Alán Aspuru-Guzik[‡] and Mircea Dincă*[†]

[†]Department of Chemistry, Massachusetts Institute of Technology, Cambridge, Massachusetts 02139, United States

[‡]Department of Chemistry and Chemical Biology, Harvard University, Cambridge, Massachusetts, 02138, United States

mdinca@mit.edu

Contents

Experimental

Materials

Starting materials were purchased from Sigma-Aldrich or TCI and used without further purification. Tris(Dibenzylideneacetone)dipalladium(0), $Pd_2(dba)_3$, was purchased from Oakwood Products, Inc. (Fluorochem Ltd.). 2,3,6,7,10,11-hexaaminotriphenylene hexahydrochloride, HATP·6HCl, was prepared according to a procedure published elsewhere.[1] Hexane, diethyl ether, ethyl acetate, toluene and silica-gel were purchased from VWR. THF was collected from an alumina column solvent purification system.

Typical synthesis of $Ni_3(HITP)_2$

A solution of 6.6 mg (0.028 mmol) of nickel chloride hexahydrate ($NiCl_2·6H_2O$) in 5 mL of water and 0.3 mL of concentrated aqueous ammonia (NH_4OH, 14 $mol·L^{-1}$) was added to a solution of 10 mg (0.019 mmol) of HATP·6HCl in 5 mL of water. This mixture was stirred in an open beaker for 2 hours at 65 °C. The resulting black powder was centrifuged, filtered, and then washed in water under reflux for a total of 36 hours (the water was refreshed 2 times during this washing step, for a total of 3 steps, 12 hours each). Finally, the solid was heated at reflux in neat acetone for another 3 h. The solid was then dried under vacuum at 150 °C. C, H, N, and Cl microelemental analysis for $Ni_3(C_{18}H_{12}N_6)_2$: Calculated: C: 54.00%; H: 3.02%; N: 20.99%; Cl: 0.00%. Found: C: 53.84%; H: 3.12%; N: 20.83%; Cl: <0.02%. A dark blue-violet film was obtained by placing a quartz substrate on a Teflon holder such that it was positioned upside-down inside the reaction vessel. The film growth was thus independent of compacting due to gravity.

Methods

Absorption spectra were taken with a CARY 5000 UV-Vis-NIR spectrophotometer.

Thermogravimetric analysis (TGA) was performed on a TA Instruments Q500 Thermogravimetric Analyzer at a heating rate of 0.5°C/min under a nitrogen gas flow of 90 mL/min on a platinum pan.

Powder X-ray diffraction (PXRD) patterns were recorded with a Bruker D8 Advance diffractometer equipped with a Göbel mirror, rotating sample stage, LynxEye detector and Cu K_α (λ = 1.5405 Å) X-ray source in a $\theta/2\theta$ Bragg-Brentano geometry. Anti-scattering incident source slit (typically 1 mm) and an exchangeable steckblende detector slit (typically 8 mm) were used. The tube voltage and current were 40 kV and 40 mA, respectively. Knife-edge attachments were used to remove scattering at low angles. Samples for PXRD were prepared by placing a thin layer of the designated materials on a zero-background silicon (510) crystal plate.

Scanning electron microscopy (SEM) images were recorded using a Leo Supra 55VP FEG SEM with an operating voltage of 3 keV.

X-ray photoelectron spectroscopy (XPS) was performed on a Thermo Scientific K-Alpha system equipped with an Al source and 180° double focusing hemispherical analyzer and 128-channel detector using a 400 µm X-ray spot size.

AFM topography images were acquired using an Asylum MFP-3D AFM system. Images were recorded in tapping mode in the air at room temperature (20–23°C) using silicon micro cantilevers (OMCL-AC200TS-*3, Olympus). The set point ratio was adjusted to 0.75–0.8 (corresponding to "light" tapping) and the scan rate was set to 0.5 Hz. Imaging was carried out in different scan directions and at different scales to verify the consistency and robustness of the evaluated structures. The thickness of films was measured by AFM profilometry.

Conductivity measurements on films were performed using the van der Pauw method under temperature control with a 4-arm Lakeshore probe station under vacuum (ca. 10^{-5} torr). Electrical measurement data were obtained using a Keithley 2400 source/meter by manually changing the probe connections. Four silver or carbon paste contacts were put on the corners of 3×3 mm^2 – 8×8 mm^2 squares of uniform film separated from the rest of the sample.

Powder conductivity were measured using a home-built press as has been described elsewhere.[2] The powder was pressed between two steel rods of 2 mm diameter inside of a glass capillary. The thickness of the powder pellets ranged from 0.1 mm to 0.5 mm.

X-ray absorption measurements were conducted on the Materials Research Collaborative Access Team (MR-CAT) beam lines at the Advanced Photon Source of Argonne National Laboratory. The Ni K edge (8333 eV) was measured on a bending magnet beam line and a spectrum of the elemental foil was collected alongside sample measurements to calibrate the energy. A water-cooled, double-crystal Si(111) monochromator was used to select the photon energies and the experiments were performed in transmission mode with argon, helium, and N_2-filled ionization chambers. Data was collected in six regions (energies relative to the elemental Ni K edge): a pre-edge region –250 to –30 eV (10 eV step size, dwell time 0.5 s), initial XANES region –30 to –12 eV (5 eV step size, dwell time –0.5s), XANES region –12 to 30 eV (1 eV step size, dwell time 1 s), an initial EXAFS region –30 eV to 6 k (0.05 k step size, dwell time 2 s), middle EXAFS region 6 k to 12 k (0.05 k step size, dwell time 4 s), and a final EXAFS region 12 k to 15 k (0.05 k step size, dwell time 8 s). The sample was prepared in an argon glove box and diluted with sufficient boron nitride to acquire an appropriate step height in the spectrum. This mixture was loaded into a 4 mm diameter cylindrical sample holder and kept under argon in a quartz tube capped with Kapton tape during the measurement. The edge energy was associated with the maximum of the first derivative of the XANES spectrum. Athena 0.8.061 was used to normalize and calibrate the data and Artemis 0.8.014 to simulate spectra of model structures determined by density functional theory. These simulations represent the sums of all calculated scattering paths.

Microelemental analyses were performed by Complete Analysis Laboratories, Inc., 1259 Route 46, Building 4C, Parsipanny, NJ 07054-4909.

Additional Figures

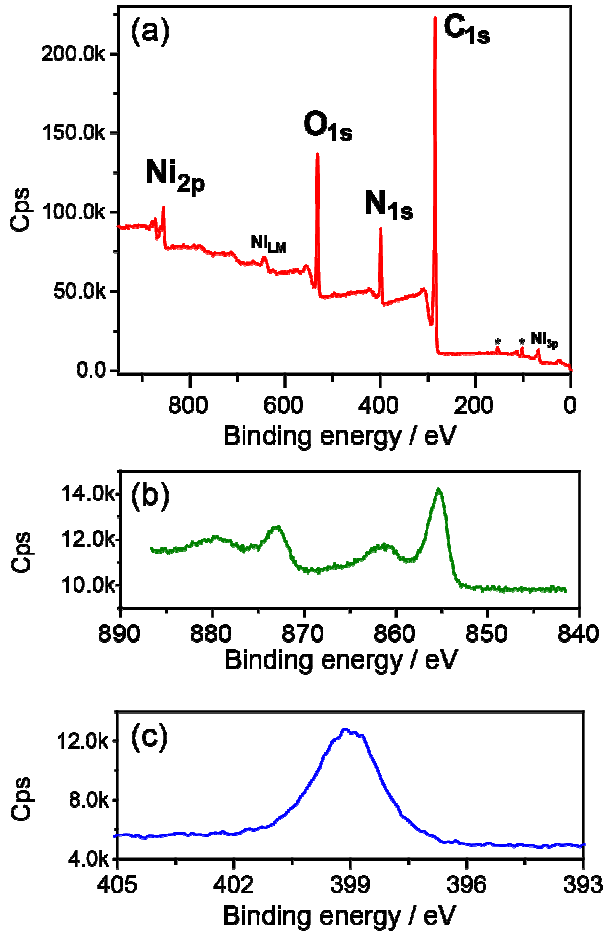

Figure S1. XPS spectra of $Ni_3(HITP)_2$ powder. (a) Energy survey spectrum, and zoom-in to the (b) Ni(2p) and (c) N(1s) energy region. Asterisks mark peaks due to Si from the substrate.

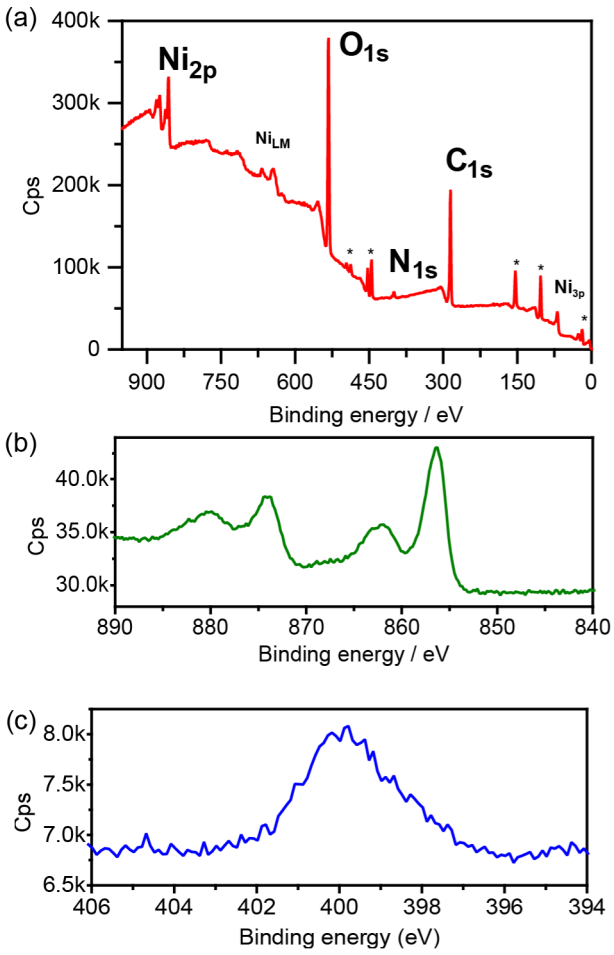

Figure S2. XPS spectra of thin $Ni_3(HITP)_2$ film (<100 nm) on ITO-coated glass slides. (a) Energy survey spectrum, and zoom-in to the (b) Ni(2p) and (c) N(1s) energy region. Asterisks mark peaks due to Si, Sn and In from the substrate.

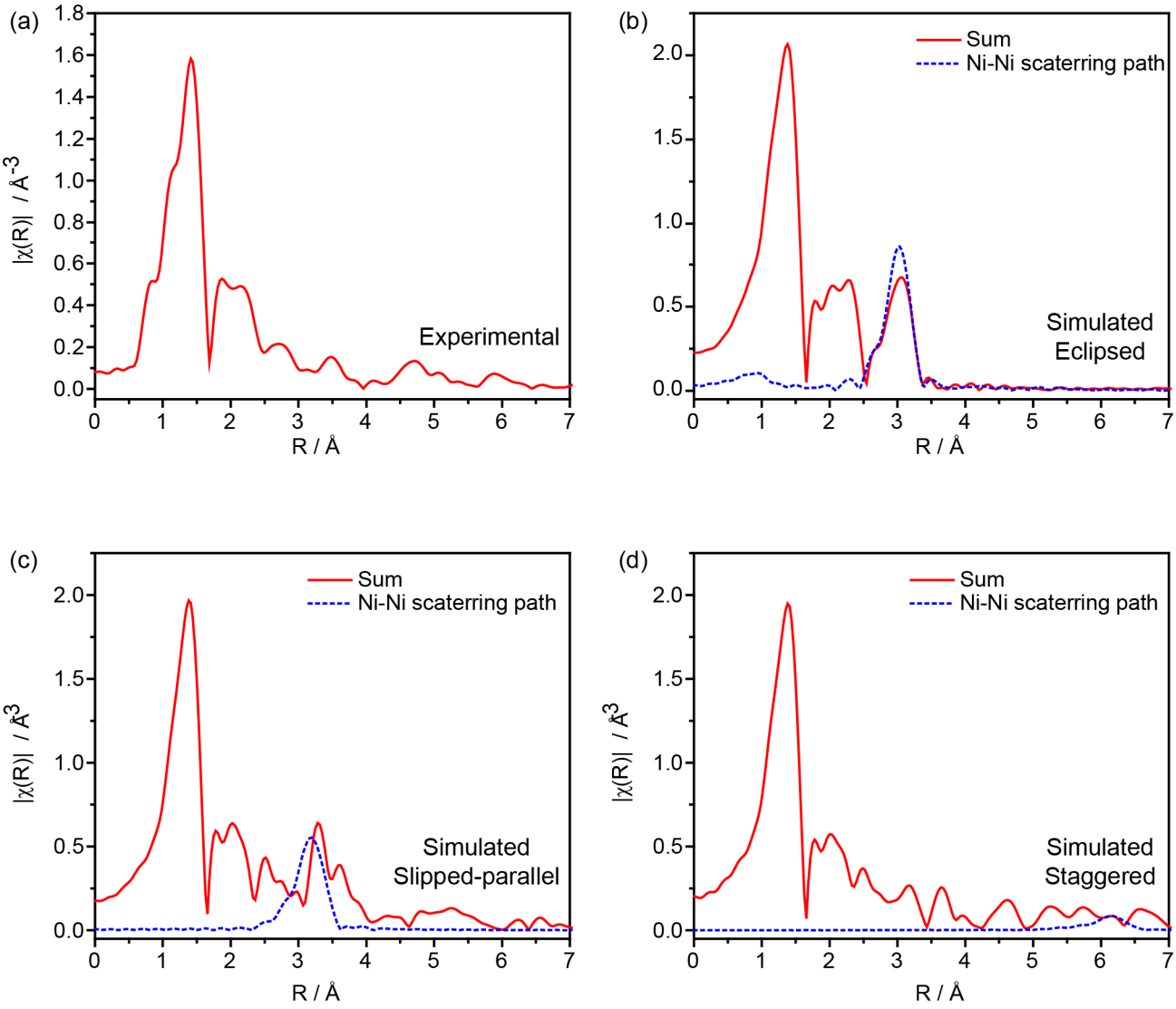

Figure S3. (a) Experimental and (b-d) simulated EXAFS data of $Ni_3(HITP)_2$ powder.

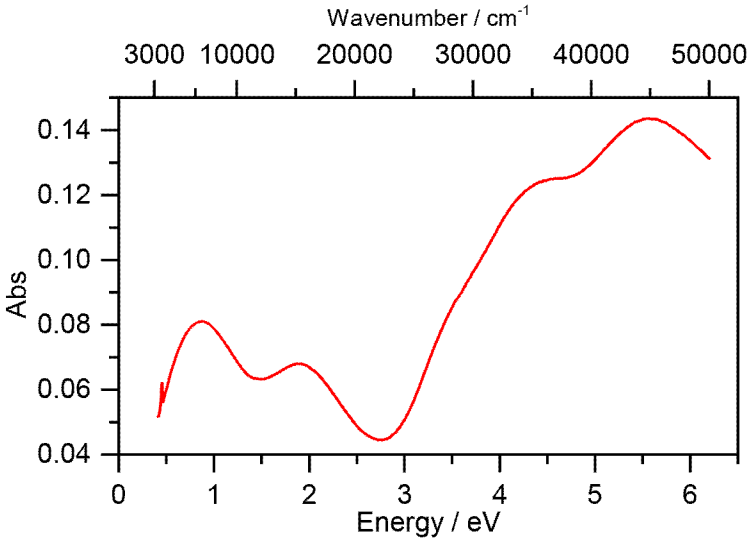

Figure S4. UV-Vis-NIR absorption of a $Ni_3(HITP)_2$ film on quartz slide.

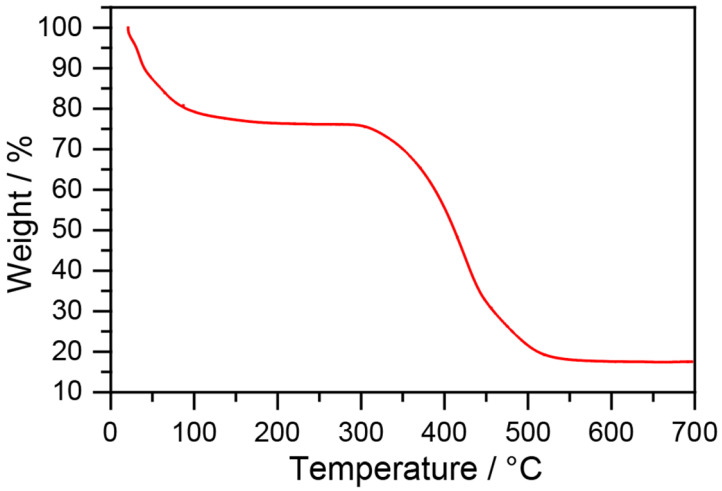

Figure S5. TGA curve of $Ni_3(HITP)_2$ powder.

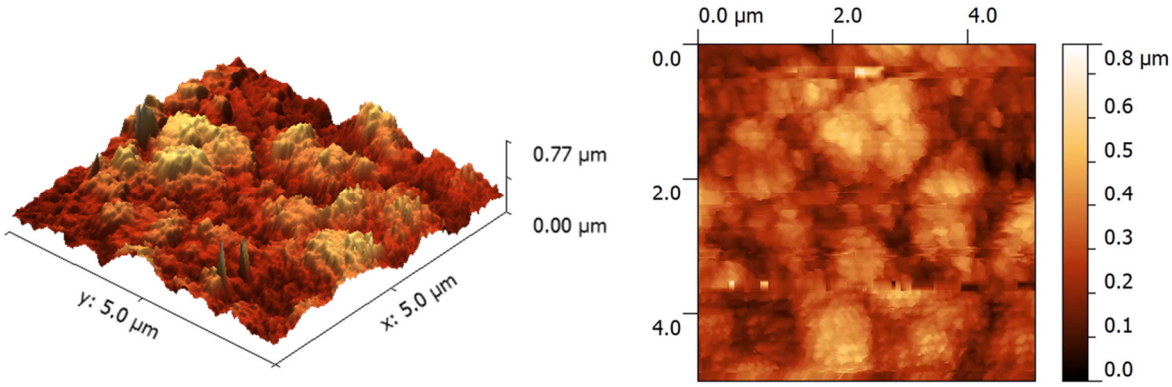

Figure S6. AFM profile image for a 500 nm $Ni_3(HITP)_2$ film on a quartz substrate.

Computational Details

The molecular fragment used to generate the model structure is shown in Figure S7. The geometry of this fragment was optimized in ORCA v3.0.1[3] using the B3LYP functional with an atom-pairwise dispersion correction with the Becke-Johnson damping scheme (D3BJ)[4] and the 6-31G(d) basis[5]. In the optimized geometry the Ni atoms formed two isosceles triangles with side lengths of 10.926 Å and 10.933 Å and angles of 59.96° and 60.02°. This structure was then converted into fractional coordinates using a cell length $a = b = 21.86$ Å, which was determined from the Ni-Ni distances of the optimized fragment. Since we do not expect an infinite 2D sheet of this material to have this squeezed angle, the unit cell was forced into P6/mmm symmetry in Avogadro v1.1.1[6] using a threshold of 1.7 pm (i.e. the maximum adjustment of any coordinate to force this symmetry was 1.7 pm). An interlayer spacing of 3.3 Å was enforced for consistency with the PXRD signal. To consider parallel-displaced structures the *c*-axis was doubled to 6.6 Å.

A total of 82 different unit cells for parallel-displaced structures were generated from the two grids of translations in the *ab*-plane shown in Figure S8. DFT single-point energy calculations were carried out on all 82 of these structures using the PBE (Perdew-Burke-Ernzerhof) exchange-correlation functional[7] with Grimme's D2 dispersion correction[8] as implemented in VASP v5.2[9]. Electron-ion interactions were described using the projector augmented wave (PAW) method[10]. A kinetic energy cutoff of 400 eV and a Γ-centered k-point mesh of $2 \times 2 \times 6$ were used for all calculations. The self-consistent energy of each of these structures was then used as a sample point for the energy of a potential energy surface that was interpolated using 2D Lagrange polynomials over a tensor product grid of Chebyshev points which were subsequently mapped back to the grid of original translations. Interpolation over the finer grid is expected to yield a more accurate representation of the potential energy surface in the region. As shown in the left-hand panel of Figure S9, the minimum of the potential energy surface corresponds to a displacement of ~1.8-1.9Å along the *a* and/or *b* axis.

We also explored the potential energy surface of the parallel-displaced structure using the Allinger MM2-1991 force field[11] as implemented in TINKER v6.3[12]. Since Ni^{II} has only been partially parameterized for this force field, we took the van der Waals parameters from Munk et al.[13] (Ni: $r_{vdw} = 1.35$ Å and $\varepsilon = 0.2$) and turned off all torsion and bond related interactions, leaving just the van der Waals and point-charge electrostatic contributions. We used a unit cell consisting of 4 layers ($c = 13.3$Å) an Ewald cutoff of 40 Å, and a particle mesh Ewald grid of $48 \times 48 \times 30$ with a maximum B-spline order of 5.

Figure S10 (left) shows the potential energy surface produced from just the van der Waals component of the MM2 energy. Figure S10 (right) shows the potential energy surface produced when an explicit charge model is added to the force field using fractional charges calculated using Breneman and Wiberg's CHELPG method[14] as implemented in ORCA with the B3LYP-D3BJ/6-31G(d). Comparing the van der Waals only MM2 result to the DFT results suggests that the PBE functional with the D2 correction is balancing the electrostatic and dispersive contributions to the energy of the layered system. When we add the explicit charge model to the MM2 calculation, we get an answer that is overly repulsive, resulting in a minimum in the potential energy surface that is inconsistent with the powder diffraction data (i.e. simulated powder spectra for structures with such large displacements are in serious disagreement with the experimental spectrum). The fact that a point charge model is overly repulsive should be expected since it is well known[15] that the quadrupole of an extended π-system can interact attractively with a cation, and thus reduce the repulsion caused by point charges.

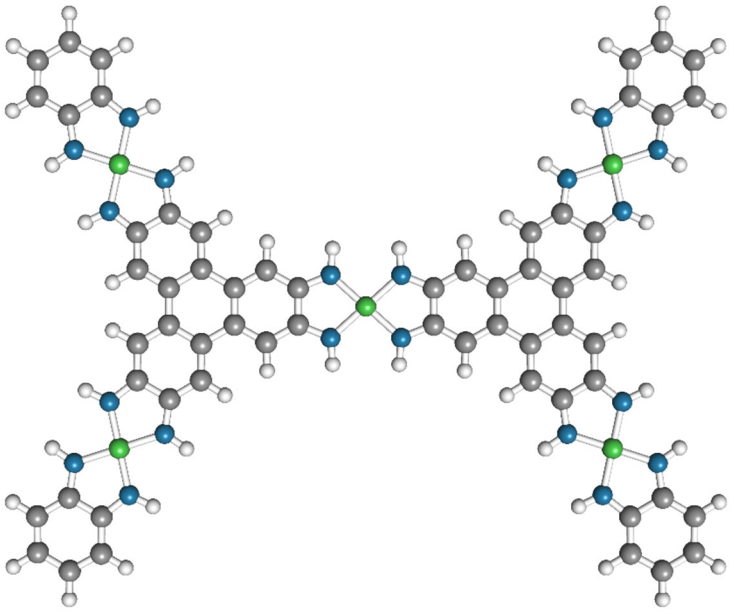

Figure S7. The hydrogen terminated fragment used to generate the model unit cell.

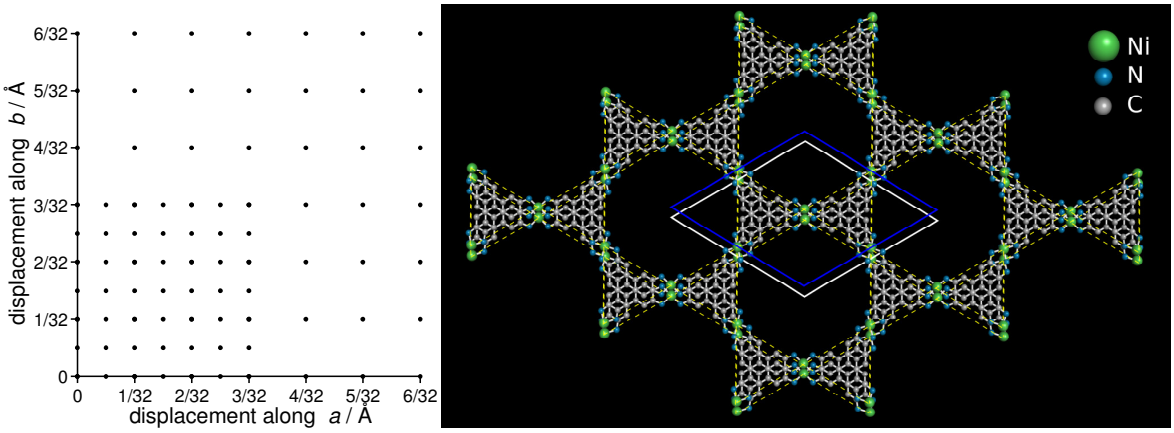

Figure S8. Left: the grids of fractional coordinate translations in the *ab*-plane that were sampled by DFT calculations. Right: example of a structure that is produced by a 1/16th displacement in both the *a* and *b* axes.

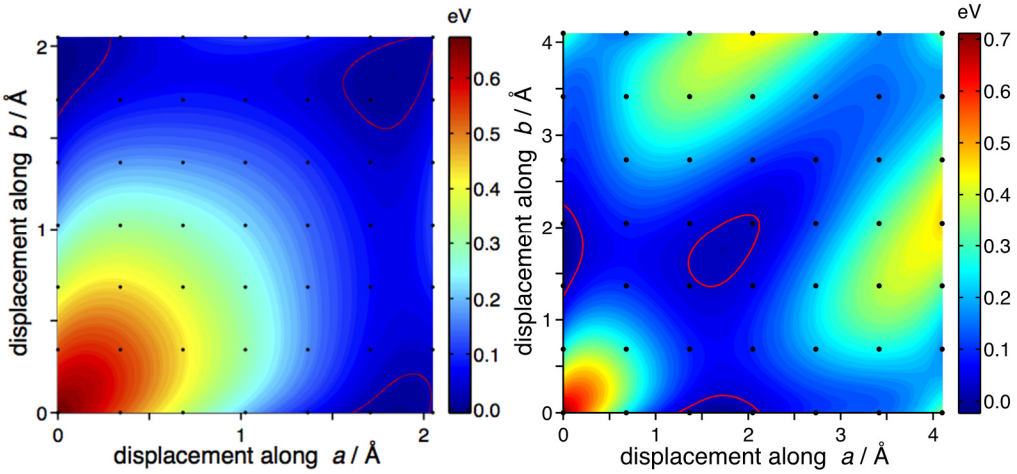

Figure S9. Contour maps of the DFT potential energy surface induced by different translations between A and B layers. Black dots correspond to locations of single-point calculations performed with the PBE-D2 functional. Red lines indicate the 'thermally accessible region' (within $k_BT \approx 0.026$ eV of the minima). The surface was produced by interpolation with 2D Lagrange polynomials on a grid of Chebyshev points. The energy is normalized to zero at the minimum. Note that the minimum obtained from the fine interpolation grid at left is closer to a displacement of ~1.8 Å in contrast to the minimum at ~1.7 Å on the larger grid.

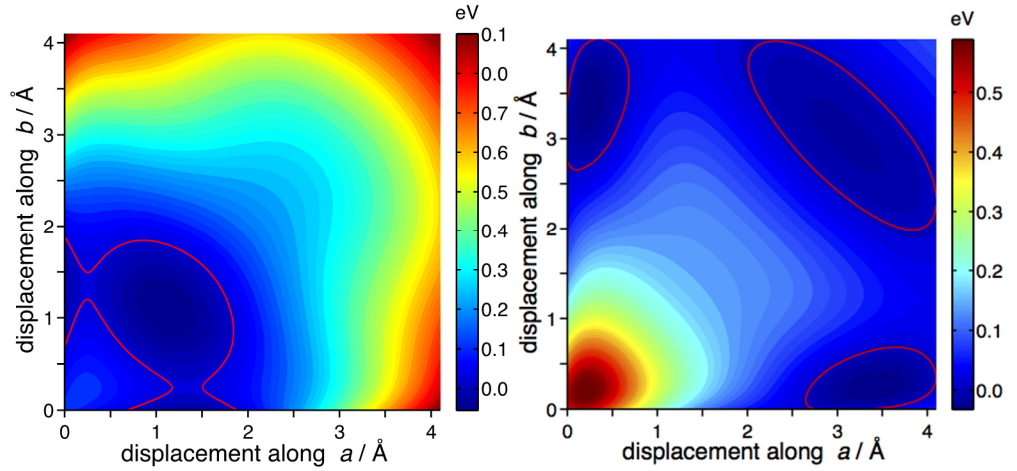

Figure S10. Contour maps of the MM2 force field potential energy surface induced by different translations between A and B. At left is just the van der Waals component of the MM2 energy. At right an explicit point charge model has been added. The point charge model is seen to be over-repulsive since the potential energy minima correspond to displacements that are inconsistent with the experimental PXRD spectrum. The thin red contour shows the 'thermally accessible region' (within $k_BT \approx 0.026$ eV of the minima). All energies have been normalized to zero.

References

(1) Chen, L.; Kim, J.; Ishizuka, T.; Honsho, Y.; Saeki, A.; Seki, S.; Ihee, H.; Jiang, D. "Noncovalently Netted, Photoconductive Sheets with Extremely High Carrier Mobility and Conduction Anisotropy from Triphenylene-Fused Metal Trigon Conjugates" *J. Am. Chem. Soc.* **2009**, *131*, 7287.

(2) Wudl, F.; Bryce, M. R. "Apparatus for two-probe conductivity measurements on compressed powders" *J. Chem. Educ.* **1990**, *67*, 717.

(3) Neese, F. "The ORCA program system" *WIREs Comput. Mol. Sci.* **2011**, *2*, 73.

(4) (a) Grimme, S.; Ehrlich, S.; Goerigk, L. "Effect of the damping function in dispersion corrected density functional theory" *J. Comput. Chem.* **2011**, *32*, 1456; (b) Grimme, S.; Antony, J.; Ehrlich, S.; Krieg, H. "A consistent and accurate ab initio parametrization of density functional dispersion correction (DFT-D) for the 94 elements H-Pu" *J. Chem. Phys.* **2010**, *132*, 154104.

(5) Hehre, W.J.; Ditchfield, R. and Pople, J. A. "Self—Consistent Molecular Orbital Methods. XII. Further Extensions of Gaussian—Type Basis Sets for Use in Molecular Orbital Studies of Organic Molecules" *J. Chem. Phys.* **1972**, *56*, 2257.

(6) Hanwell, M. D.; Curtis, D. E.; Lonie, D. C.; Vandermeersch, T.; Zurek, E. and Hutchison, G. R. "Avogadro: An advanced semantic chemical editor, visualization, and analysis platform" *J. Cheminformatics* **2012**, *4*, 17.

(7) Perdew, J. P.; Burke, K. and Ernzerhof, M. "Generalized gradient approximation made simple" *Phys. Rev. Lett.* **1997**, *77*, 3865.

(8) Grimme, S. "Semiempirical GGA-Type Density Functional Constructed with a Long-Range Dispersion Correction" *J. Comput. Chem.* **2006**, *27*, 1787.

(9) (a) Kresse, G.; Furthmuller, J. "Efficiency of ab-initio total energy calculations for metals and semiconductors using a plane-wave basis set" *Comput. Mater. Sci.* **1996**, 6, 15; (b) Kresse, G.; Hafner, J. "Ab initio molecular dynamics for liquid metals" *Phys. Rev. B* **1993**, *47*, 558; (c) Kresse, G.; Hafner, J. "Ab initio molecular-dynamics simulation of the liquid-metal–amorphous-semiconductor transition in germanium" *Phys. Rev. B* **1994**, *49*, 14251.

(10) (a) Kresse, G.; Joubert, D. "From ultrasoft pseudopotentials to the projector augmented-wave method" *Phys. Rev. B* **1999**, *59*, 1758; (b) Blochl, P. E. "Projector augmented-wave method" *Phys. Rev. B* **1994**, *50*, 17953.

(11) Allinger, N. L. "Conformational Analysis 130. MM2. A Hydrocarbon Force Field Utilizing V1 and V2 Torsional Terms" *J. Am. Chem. Soc.* **1997**, *99*, 8127-8134.

(12) Ponder, J. W.; Richards, F. M. "An efficient newton-like method for molecular mechanics energy minimization of large molecules" *J. Comput. Chem.* **1987**, 8, 1016.

(13) Munk, V. P.; Cham, S. T.; Fenton, R. R.; Hocking, R. K.; Hambley, T. W. "Insights into the van der Waals Radius of Low-Spin Ni(II) from Molecular Mechanics Studies and the Crystal Structures of [Ni(cis-cyclohexane-1,3-diamine)$_2$]Cl$_2$, [Ni{(R)-5,5,7-trimethyl-1,4-diazacycloheptane}$_2$]Cl$_2$·H$_2$O and [Ni(5,7-dimethyl-1,4-diazacycloheptane)$_2$](ClO$_4$)$_2$. Synthesis of 5,7-Dimethyl-1,4-diazacycloheptane and an Improved Synthesis of cis-Cyclohexane-1,3-diamine" *Aust. J. Chem.* **2002**, *55*, 523-529.

(14) Breneman, C. M.; Wiberg, K. B. “Determining atom-centered monopoles from molecular electrostatic potentials. The need for high sampling density in formamide conformational analysis” *J. Comp. Chem.* **1990**, 11, 361.

(15) Dougherty, D. A.; Ma, J. C. “The Cation-π Interaction” *Chem. Rev.* **1997**, *97*, 1303.